Journal of Applied Polymer Science

Microstructural Characteristics and Crystallization Behaviors of Poly(L-lactide) Scaffolds by Thermally Induced Phase Separation

Liumin He, Qinhua Zuo, Yunfeng Shi, Wei Xue

Department of Biomedical Engineering, College of Life Science and Technology, Jinan University, Guangzhou, 510632 China

Correspondence to: L. He (E-mail: jnulmhe@gmail.com) or W. Xue (E-mail: weixue_jnu@yahoo.com.cn)

ABSTRACT: In this study, poly(L-lactic acid) (PLLA) was prepared by four typical approach systems, namely, solid–liquid phase-separation processes from PLLA–dioxane at −80°C, PLLA–dioxane–water at −80°C, PLLA–tetrahydrofuran (THF) at −80°C, and PLLA–THF at 18°C. The microstructural characteristics and crystallization behaviors of PLLA were investigated by scanning electron microscopy, differential scanning calorimetry, X-ray diffraction, and Fourier transform infrared spectroscopy. In the PLLA–dioxane binary system and PLLA–dioxane–water ternary system, the solvent froze immediately after quenching to a low temperature, and this restricted the PLLA chain arrangement. Thus, the PLLA amorphous phase dominated in the scaffolds, and solid-walled structures were produced. THF was liquid throughout the entire process, which enabled free PLLA chain arrangement and further crystallization. Single crystals aggregated by crystal nucleation and growth at a critical temperature (T_c) of 18°C; this resulted in its most common and stable polymorph, the α form. However, α′-form crystals, which were assumed to be limit-disordered crystals of the α form, were produced at a low T_c (−80°C). Scaffolds with a plateletlike structure were produced at a T_c of 18°C, whereas a nanofibrous network was obtained at −80°C. PLLA crystallization competed with phase separation; thus, the crystal structure and scaffold morphology depended on the codevelopment of these two processes. Finally, the effects of the scaffold morphologies on the cell behaviors were studied, and the nanofibrous scaffold was found to have better cell adhesion and viability than the other three scaffolds. © 2013 Wiley Periodicals, Inc. J. Appl. Polym. Sci. **2014**, *131*, 39436.

KEYWORDS: biomaterials; differential scanning calorimetry (DSC); manufacturing; structure–property relations

Received 5 July 2012; accepted 16 April 2013

DOI: 10.1002/app.39436

INTRODUCTION

Thermodynamic demixing occurs when a homogeneous polymer–diluent system is quenched or upon exposure of a mixture to an additional nonsolvent, which converts to binary phase regions composed of polymer-rich and polymer-poor phases. According to the thermodynamic state in which the polymeric solution is converted, two phase-separation mechanisms may be involved, namely, solid–liquid (S–L) and liquid–liquid (L–L) phase separation. A typical schematic of the temperature–composition phase with an upper critical solution temperature is presented in Figure 1 to elucidate the mechanism of thermally induced phase separation (TIPS). When the quenching end temperature is located between the critical temperature (T_c) and the solvent freezing point (T_f) with $T_c > T_f$, L–L phase separation occurs and is identified as either binodal demixing, spinodal decomposition, or a combination of both.[1] The solution separates into polymer-rich and polymer-poor phases upon entering the metastable region between the spinodal and binodal lines by a nucleation and growth mechanism. If the unstable area below the spinodal line is entered, phase separation occurs through spinodal decomposition, and this results in bicontinuous polymer-rich and polymer-poor phases.[2] However, the polymer–diluent system undergoes S–L phase separation when $T_c < T_f$, whereas the solvent is completely solidified before L–L phase separation.[3,4]

The subsequent solvent removal of the phase-separated polymer solution from the TIPS system can produce porous structures. The morphology of the resultant scaffolds depends on the mechanisms of phase separation. The metastable region leads to a beadlike or poorly interconnected closed pore structures for polymer concentrations lower or higher than the critical point concentration,[5–7] whereas spinodal phase separation results in a highly interconnected structure.[8–10] S–L phase separation produces bundles of channels or anisotropic ladderlike structures because of a preferential orientation induced by the progress of the crystallization front line of the solvent, for example, dioxane.[11] The resulting morphology can be controlled by various experimental parameters, including the polymer concentration, quenching temperature, quenching rate, quenching period or aging time, solvent-to-nonsolvent ratio, and surfactant or porogen addition.[12,13]

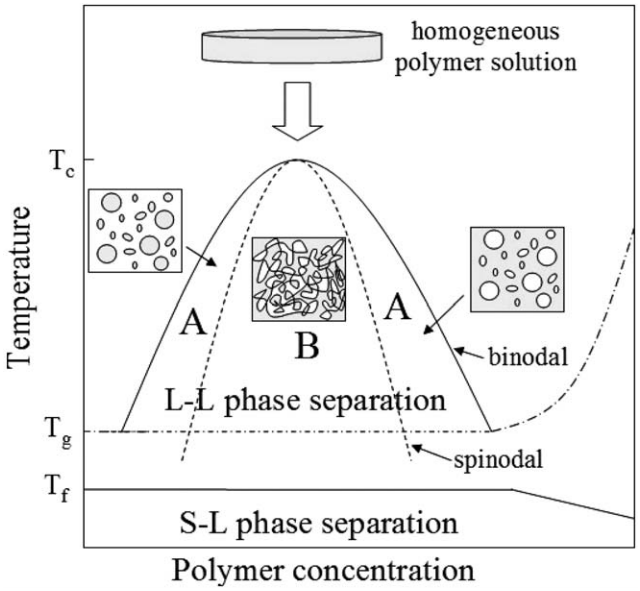

Figure 1. Schematic of the temperature–composition phase diagram of the polymer solution: A, metastable region; B, unstable region; T_c, critical temperature of L–L phase separation; T_g, glass-transition temperature of the polymer solution; T_f, freezing point of the solvent.

For semicrystalline polymers, phase separation is usually accompanied by simultaneous or subsequent polymer crystallization. In many cases, these two processes compete with each other because both are thermodynamically driven processes, and the scaffold morphologies vary because of different mechanisms.[14] Apart from solid-walled pores, spinodal L–L phase separation produces nanofibers because of the consequential crystallization of the polymer-rich phase. As a semicrystalline polymer, poly(L-lactic acid) (PLLA) was used to prepare a three-dimensional (3D) fibrous network with nanoscale fiber diameters by L–L phase separation from a PLLA–tetrahydrofuran (THF) solution at a high quenching rate. However, plateletlike structures are usually produced because of the aggregation of single crystals through crystal nucleation and growth with increasing quenching temperature, which indicates a slow quenching rate.[15] A similar phenomenon was detected in our previous study when we prepared PLLA nanofibrous scaffolds from a ternary polymer–dioxane–water system.[16] In this approach, the gelation of the system caused by PLLA microcrystallinity crucially influenced the morphology of the resulting scaffolds. Therefore, both the phase separation and polymer crystallization should be considered in nanofibrous scaffold fabrication by TIPS. Systematic investigations of the crystallization behaviors of PLLA scaffolds prepared by various TIPS technologies can enable a thorough understanding of the mechanisms of TIPS and its scaffold morphology formation. However, such investigations are limited.

Meanwhile, crystallization plays an important role in the bulk properties of semicrystalline polymers. Although PLLA crystallization behaviors have been widely studied, most studies have focused on solution-cast films that do not have the morphology commonly used in tissue engineering applications. PLLA crystallization behaviors must be examined in the state of its applications. Thus, in this study, we aimed to investigate the crystallization of PLLA scaffolds prepared by TIPS with PLLA–dioxane, PLLA–dioxane–water, and PLLA–THF; these are commonly used to prepare 3D scaffolds for tissue engineering. IR spectroscopy is sensitive to the conformation and local molecular environment of polymers and can provide considerable information on the chain conformation, crystallinity, and phase transformation.[17] Therefore, in addition to differential scanning calorimetry (DSC) and X-ray diffraction (XRD), Fourier transform infrared (FTIR) spectroscopy was used in this study to elucidate the crystallization behaviors of PLLA at the molecular scale.

Although many investigations have been conducted on PLLA scaffolds prepared by TIPS for tissue engineering applications, no systematic studies on the effects of the scaffold morphology on the cell behavior have been conducted. Therefore, in this study, we also investigated the effects of the four typical morphologies of PLLA scaffolds prepared by TIPS on the cell behavior.

EXPERIMENTAL

PLLA, with a molecular weight of 300,000 Da, was purchased from Polysciences, Inc. All reagents were used as obtained without further treatment.

Four PLLA scaffolds were fabricated by a commonly used TIPS approach from PLLA–dioxane, PLLA–THF binary systems, and a PLLA–dioxane–water ternary system, which are listed in Table I.

For specimens A and B, certain amounts of PLLA were dissolved in dioxane (A) and dioxane/water (87/13 w/w; B), respectively, at 65°C to produce a 4% w/v solution. Then, the samples were rapidly quenched to −80°C and annealed for 2 h. The scaffolds were finally obtained after freeze drying followed by further vacuum drying to thoroughly remove the solvents.

For specimens C and D, a certain amount of PLLA was dissolved in THF at 65°C to produce a 4% w/v solution. Then, the samples were quenched to −80°C (C) and 18°C (D), respectively, and annealed for 2 h. THF was leached out by the placement of the samples in deionized water at 4°C, with the water changed three times a day. After that, the samples were frozen, and the scaffolds were finally obtained after freeze drying.

The morphologies of various PLLA scaffolds prepared by TIPS observed under scanning electron microscopy (SEM; JSM-TE300, JEOL, Japan) with an accelerating voltage of 20 kV. Before observation, the samples were coated with gold using a sputter coater (JEOL JFC-1200 fine coater, Japan).

Table I. 4% w/v PLLA 3D Scaffolds as Prepared by TIPS from Different Solvent Systems and Quenching Temperatures

PLLA scaffold	Solvent	Quenching temperature (°C)
A	Dioxane	−80
B	Dioxane–water (87/13 w/w)	−80
C	THF	−80
D	THF	18

The thermal properties of the samples were analyzed by DSC (DSC 204 F1 Phoenix, Netzsch-Gerätebau GmbH) in a temperature range from 20 to 220°C at a heating rate of 10°C/min. The first heating was performed for the analysis.

The crystal of the PLLA scaffold was characterized by XRD (D/MAX 2200 VPC, Rigaku, Ltd., Japan) with a Cu Kα source. The analysis was performed in the 2θ range of 10–35° at a scanning rate of 1.5°/min.

The FTIR spectrum was measured with a Vertex 70 spectrometer (Bruker). An attenuated total reflectance module was coupled to the FTIR spectrometer for the recording of the attenuated total reflectance–FTIR absorbance spectra in the range between 4000 and 400 cm^{-1}.

NIH-3T3 cells (from a mouse embryonic fibroblast cell line) were cultured in Dulbecco's modified Eagle's medium (Gibco) supplemented with 10% fetal bovine serum (Gibco) and 1% penicillin–streptomycin (Gibco) at 37°C at 5% CO_2 unless otherwise indicated. The NIH-3T3 cells were seeded on scaffolds at a density of 1.0×10^4 cells/mL for 2 days. Then, MTS assay (CellTiter 96® AQueous One Solution Cell Proliferation Assay) reagent was added to the cell-seeded scaffold complex at a ratio of 1:5 of MTS to medium; the cells were then cultured for another 4 h. Thereafter, aliquots of 120 μL were pipetted into the wells of a 96-well plate and placed in a spectrophotometric plate reader (ELX800, Bio-Tek), and the absorbance at 490 nm for each well was measured. To investigate the cell morphologies, the cells were fixed in 3.7% paraformaldehyde for 30 min at room temperature after 2 days, rinsed three times in phosphate-buffered saline solution (5 min each), then dehydrated in a graded series of ethanol, and kept in a fume hood to air dry. The cell morphologies were observed with SEM (JSM-TE300, JEOL, Japan).

Statistical analysis was performed with SPSS statistical software (SPSS 11.0). The differences between the groups were assessed with the analysis of variance test. The results were considered statistically significant when the p value was <0.05.

RESULTS AND DISCUSSION

PLLA is extensively used to fabricate scaffolds by TIPS for various engineering applications in tissues such as bone, nerve, and cartilage. According to the different mechanisms of phase separation, scaffolds of various morphologies can be obtained. The four most typical ones are presented in Figure 2; these include an anisotropic ladderlike structure [Figure 2(A)], interconnected porous structure [Figure 2(B)], nanofibrous network [Figure 2(C)], and plateletlike structure [Figure 2(D)]. Given the high freezing point (11.8°C) of dioxane, it crystallizes during quenching and undergoes S–L phase separation. The ultimate scaffold structure has been determined by the forward progress of the crystallization of the solvent.[11,18] An interconnected porous structure typical of L–L phase separation resulted from the PLLA–dioxane–water (dioxane–water = 87/13 w/w) ternary system even under the same fabrication conditions used for specimen A. The gradual addition of water increased the cloud point and decreased the freezing point of the solution and thereby extended the time window within which the system was located in the unstable region of L–L phase separation.[18] A nanofibrous network and plateletlike structure were obtained from the PLLA–THF binary system at different quenching temperatures. Because the quenching end temperatures (−80 and 18°C) were above the freezing point of THF (−108.5°C), THF was a liquid throughout the entire process. Therefore, the PLLA molecular chain had the time and freedom to arrange, becoming microcrystalline and leading to the apparent gelation of the systems. However, a higher gelation temperature produced a

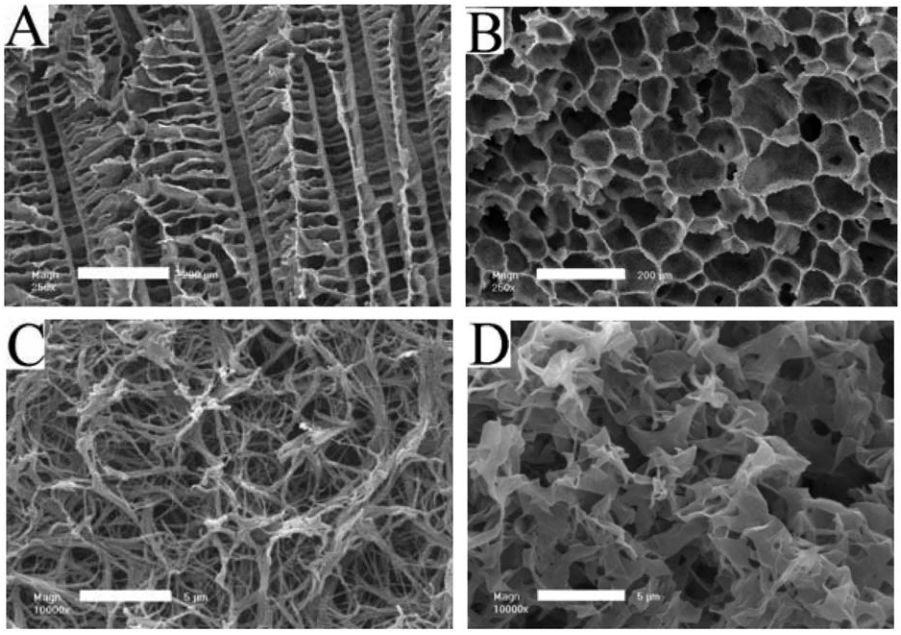

Figure 2. SEM images of the 4% (w/v) PLLA 3D scaffolds prepared by TIPS from systems A to D: Scale bars: (A,B) 200 and (C,D) 5 μm.

plateletlike structure instead of nanofibers. Nanofibers were hypothesized to be formed by the spinodal L–L phase separation of the polymer solutions and the consequential crystallization of the polymer-rich phase, whereas the plateletlike structure was formed by the aggregation of many single crystals through a crystal nucleation and growth mechanism.[15,16]

The thermal properties of the scaffolds prepared by the four TIPS methods were studied with DSC thermograms, as shown in Figure 3. Two broad exotherms ascribed to cold crystallization with minima at 129.4 and 127.6°C were observed in the scans of specimens A and B, respectively, whereas exotherms were absent in the scans of specimens C and D. Therefore, unstable and imperfect crystals were formed in specimens A and B; these crystals further reorganized during cold recrystallization. Melting occurred between 170 and 187°C above the cold crystallization, and single-endothermic peaks were found in specimens A and B. However, a peak at 179.0°C, indicated by asterisk in the curve, appeared before the final melting peak at 182.0°C in specimen C. A peak with a higher magnitude but a lower temperature than specimen C was observed in specimen D. The double-melting behavior of PLLA was reported previously, and different mechanisms have been proposed to explain the multiple melting behaviors of polymers. Yasuniwa et al.[19] ascribed it to the melt-recrystallization behavior. The low-temperature melting endotherm was attributed to the primary crystallites formed during fabrication, whereas the high-temperature one reflected the relatively perfect lamellar stacks caused by recrystallization during the DSC heating scan.[20]

On the basis of the DSC results, the thermal parameters of the PLLA scaffolds, including the cold-crystallization temperature (T_{cc}), cold-crystallization enthalpy (ΔH_{cc}), melting temperature (T_m), melting enthalpy (ΔH_m), and total enthalpy ($\Delta H = \Delta H_m + \Delta H_{cc}$), were evaluated and are summarized in Table II. The positive values of ΔH for all of the samples indicated that PLLA homocrystallites were formed in the scaffolds during fabrication by TIPS. However, a very low ΔH was obtained in specimen A; this indicated that the amorphous phase predominantly developed during scaffold fabrication and the crystallites were mainly formed during the DSC heating scan. A much lower ΔH_{cc} was obtained in specimen B; this resulted in a higher ΔH of the resulting scaffold. Higher ΔH_m values compared to those of specimens A and B were observed in the DSC curves of specimens C and D, and no cold-crystallization thermogram was identified. This finding indicated that a higher crystallinity was created in specimens C and D. On the basis of the aforementioned analysis, S–L phase separation occurred during the fabrication of specimen A, whereas L–L phase separation occurred in the fabrication of specimens B, C, and D. Dioxane immediately froze after the binary PLLA–dioxane system was quenched to a temperature significantly lower than the freezing point of dioxane; this restricted the arrangement of PLLA chains and resulted in a low crystallinity. The addition of water induced an L–L phase separation before the solvent froze, and a time window was created for PLLA chain arrangement. The time window was extended in systems C and D. Furthermore, THF was in liquid form throughout the entire process; thus, PLLA chain arrangement was much easier in systems C and D than in systems A and B.

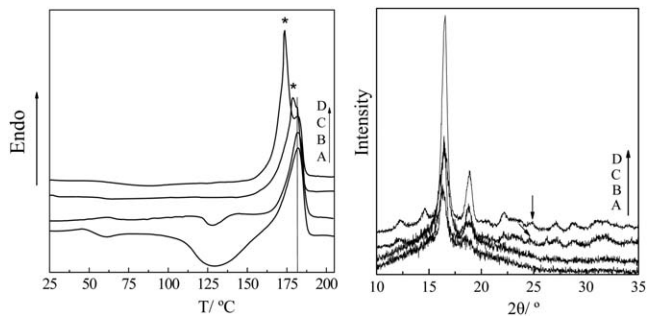

Figure 3. DSC thermograms (left) and XRD diagrams (right) of the 4% (w/v) PLLA 3D scaffolds prepared by TIPS from systems A to D. T is defined as temperature and 2θ is defined as diffraction angle.

Table II. Thermal Properties of the 4% w/v PLLA 3D Scaffolds as Prepared by TIPS from the Systems of A, B, C, and D Determined by DSC

PLLA scaffold	T_{cc} (°C)	ΔH_{cc} (J/g)	T_m (°C)	ΔH_m (J/g)	ΔH (J/g)
A	129.4	−45.1	182.3	53.9	8.8
B	127.6	−5.8	181.8	43.9	38.1
C	—	—	179.0/182.0	53.9	53.9
D	—	—	173.5/182.3	70.4	70.4

$\Delta H = \Delta H_m + \Delta H_{cc}$.

As a semicrystalline polymer, PLLA can crystallize into three different crystal modifications, namely, α, β, and γ forms, according to the processing conditions. Recently, a new crystal form, PLLA α'-form crystals, has been proposed to be a limit-disordered crystal with the same 10_3 conformation as the α form but a loose packing manner.[21] The crystalline structure of PLLA scaffolds prepared by different TIPS approaches was investigated by XRD, and the results are shown in Figure 4. For all of the scaffolds prepared by TIPS, the two strongest reflections, (200)/(100) and (203), were observed at about 16.3 and 18.7°, respectively. Several weak diffraction peaks located at 2θ = 12.1, 14.4, 22.2, and 28.5°, belonging to the reflections at 004/103, 010, 015, and 300, respectively,[22,23] were detected in the diffraction curve of specimen D but not in those of specimens A, B, and C. Moreover, a characteristic peak situated at $2\theta \approx 24.5°$ (indicated by arrows) was observed in the curves of specimens C and D but not in those of specimens A and B. The characteristics of the XRD pattern of specimen D, which was the scaffold fabricated from PLLA–THF at a quenching temperature of 18°C, agreed well with the orthorhombic crystal structure of the α-form modification,[24] whereas the peak at $2\theta \approx 24.5°$ was the characteristic reflection of the α' form.[23] Therefore, we speculated that α- and α'-form mixed crystals were produced in specimen D, whereas the α' form was mainly produced in specimen C. The size of the PLLA crystallites calculated according to the Scherrer formula increased in the order A < B < C < D (Figure 4). Moreover, a sudden increase in the crystallite size was found in specimen D compared with the other three specimens. Similar results were obtained in our previous study when we prepared PLLA scaffolds by L–L phase

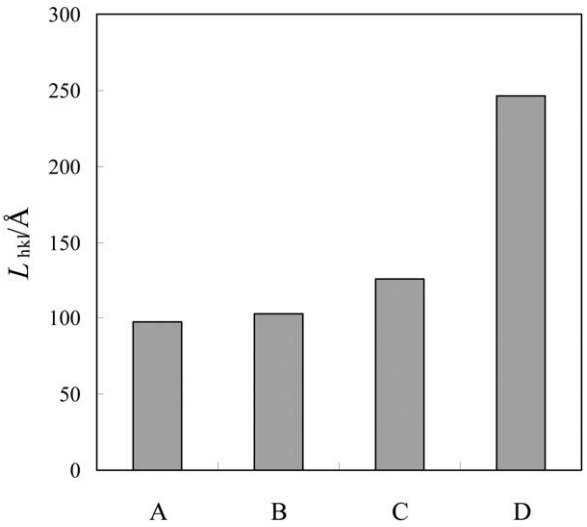

Figure 4. PLLA crystallite size in the scaffold prepared by TIPS from systems A to D. L_{hkl} is defined as the size of crystallites calculated according to Scherrer formula.[16]

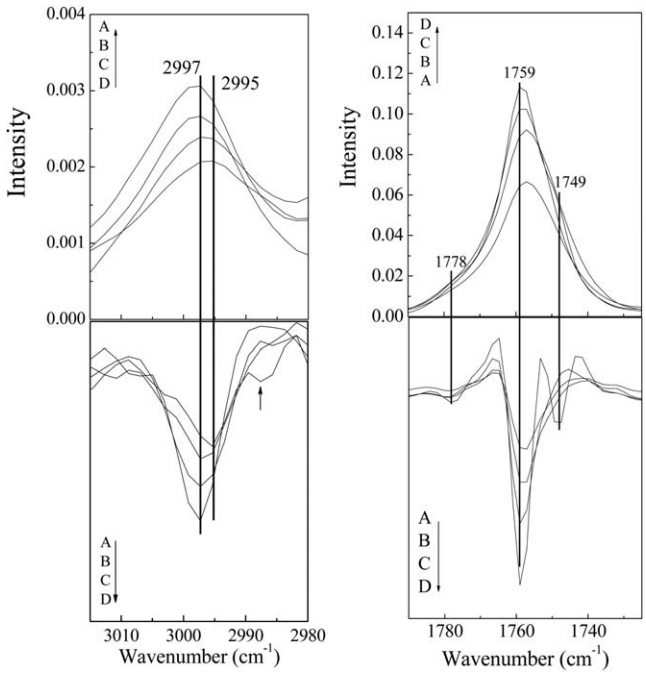

Figure 5. IR spectra (top) and second derivative spectra (bottom) of the PLLA scaffolds prepared by TIPS from the various systems listed in Table I from 3015 to 2985 cm^{-1} and 1790 to 1735 cm^{-1}.

separation from a ternary polymer–solvent system at high gelation temperatures. This similarity was attributed to lamellar thickening and crystal perfecting.[16] Therefore, apart from the melt recrystallization revealed by DSC analysis, multiple lamellae and multiple crystal structures may explain the multiple melting behaviors of PLLA.[23]

FTIR spectroscopy is widely used to analyze and identify material structures and is being increasingly adopted to elucidate crystalline structure and behavior. FTIR spectroscopy is sensitive to the molecular conformation, interaction, and the local chemical/physical environment of polymers and can thus provide considerable information on semicrystalline polymers, including chain conformations, crystallinity, and phase transformations.[17] In this study, the crystallization behaviors of PLLA scaffolds prepared by TIPS were investigated by the identification of the characteristic bands sensitive to the crystallization of PLLA during TIPS. The bands assigned to the CH_3 asymmetric stretching mode [$\nu(CH_3)$] from 3015 to 2985 cm^{-1} and the second derivative spectra are shown in Figure 5. The band at 2997 cm^{-1} assigned to the $\nu(CH_3)$ mode of the crystalline component was detected in the IR spectra of specimens B, C, and D but not in that of specimen A; this showed a band at 2995 cm^{-1}. Zhang et al.[25] ascribed the band at 2995 cm^{-1} to the PLLA crystalline component in one of their studies but to the PLLA amorphous phase in another study.[17] In this study, this band was ascribed to the amorphous phase because another band assigned to the PLLA amorphous phase appeared at 2986 cm^{-1} in the spectrum of specimen A, as indicated by the arrow. The C═O stretching band [ν(C═O)], as a localized vibrational mode, is an important band because it is almost uncoupled from the vibrational modes of the chain skeleton and well resolved in the IR spectrum. Two splitting bands at 1778 and 1749 cm^{-1} appeared in the spectrum of specimen D but not in those of the other specimens. According to previous studies, the IR bands at 1778, 1759, and 1749 cm^{-1} are characteristic of the α-form PLLA, whereas the band at 1757 cm^{-1} corresponds to the amorphous phase.[21,26] Our results indicate that α-form crystals were predominantly developed in specimen D by L–L phase separation from the PLLA–THF binary system, more significantly at a gelation temperature of 18°C. These results were consistent with the XRD results. By contrast, the amorphous phase predominantly developed in specimens A and B by S–L phase separation from the PLLA–dioxane binary system and by L–L phase separation from the PLLA–dioxane–water ternary system.

The FTIR spectra and corresponding second-derivative spectra of various PLLA scaffolds from 1500 to 700 cm^{-1} are shown in Figure 6. Compared with specimens A, B, and C, the splitting bands at 1200 and 1222 cm^{-1}, assigned to ν_{as}(C—O—C) + $r_{as}(CH_3)$, and at 1053 cm^{-1}, assigned to [ν(C—CH_3)] (indicated by arrows), were only detected in the spectrum of specimen D. All of these bands were associated with the intermolecular and intramolecular interactions in the crystalline phase. Notably, a clear band assigned to the coupling of C—C stretching and CH_3 rocking was present at 922 cm^{-1} in the spectrum of specimen D. According to a previous study, the 922-cm^{-1} peak was characteristic of α-form crystals and was very sensitive to the 10_3 helical chain conformation of PLLA.[27] Given that all of the aforementioned bands were characteristic of α-form PLLA combined with the bands of ν(C═O) and $\nu(CH_3)$, PLLA α-form crystals probably predominantly developed in specimen D, which was fabricated by L–L phase separation from the PLLA–THF binary system at a quenching temperature of 18°C. However, determining the existence of PLLA α′-form crystals in the scaffolds was difficult because of the complexity of the fingerprint bands and the highly spectral overlapping, although the characteristic band of the α′ form at 1761 cm^{-1}, assigned to ν(C═O), was absent in the spectra.

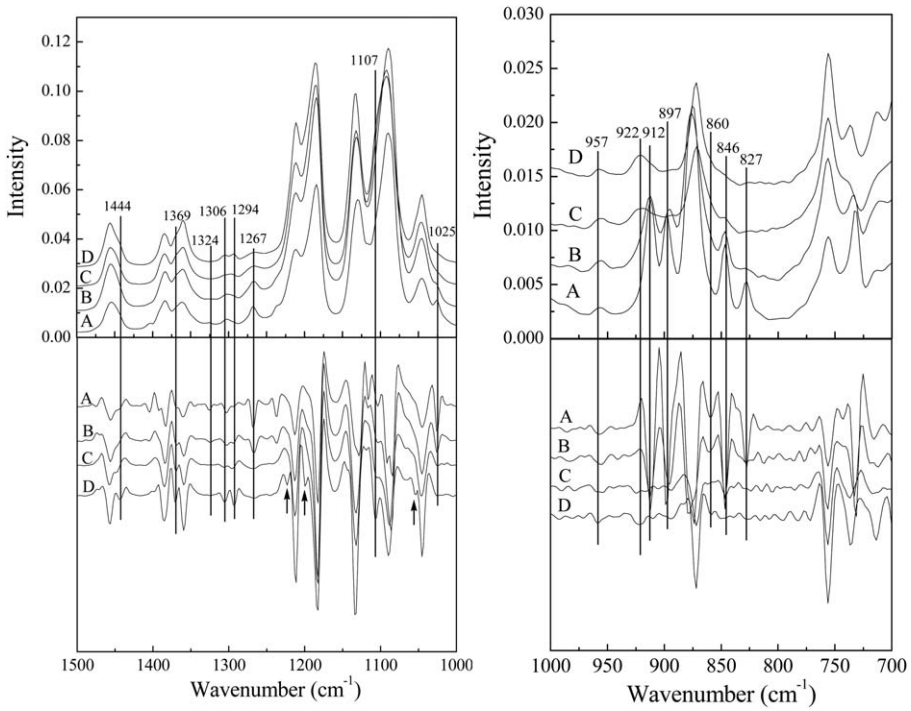

Figure 6. IR spectra (top) and second derivative spectra (bottom) of the PLLA scaffolds prepared by TIPS from the various systems listed in Table I from 1500 to 700 cm^{-1}.

By contrast, the splitting bands typically ascribed to the PLLA amorphous phase were present in the spectra of specimens A and B but were absent in those of specimens C and D; these included the bands at 1267, 1025, 912, 897, 860, and 846 cm^{-1}. Therefore, the PLLA amorphous phase dominated specimens A and B. Sawai et al.[28] and Pan et al.[29] reported that the band at 912 cm^{-1} belonged to the CH_3 rocking mode for β crystals.[28,29] However, the corresponding diffraction peak of the 003 plane of the PLLA β-form crystals located around $2\theta = 30.0°$ was not observed in the XRD patterns of specimens A and B. The intensities of several crystalline-sensitive bands of $\delta_{as}(CH_3)$ at 1444 cm^{-1} and $\delta(CH)$ + CH wagging at 1369, 1207, and 1294 cm^{-1} were found to change in the sequential order D > C > B > A. Meanwhile, the wave numbers shifted toward higher ones when specimens A and B were compared with specimens C and D. For example, the bands in specimens A and B appeared at 1302, 1103, and 732 cm^{-1}, whereas the bands in specimens C and D were located at 1306, 1107, and 738 cm^{-1}, respectively. These results indicated that higher crystallinity developed in specimens C and D than in specimens A and B; this was in agreement with the aforementioned analysis that a significant amount of crystallinity and more perfect crystals were produced in specimens C and D than in specimens A and B. This result was attributed to the significantly lower freezing point of THF compared to those of dioxane and water, which resulted in more time for PLLA chain arrangement and crystallization.

To examine the influence of the PLLA scaffolds with four characteristic morphologies (viz., anisotropic ladderlike structures, round pores, nanofibrous structures, and microscaled plateletlike lamellae) on the cell adhesion and viability, NIH-3T3 cells were cultured in the scaffolds for 2 days. The cell morphologies on different scaffolds were investigated by SEM. Figure 7 shows that cells adhered well onto all of the PLLA scaffolds prepared by TIPS from various systems, and cell spreading was observed. However, cells adhered only to the surfaces of specimens A, B, and D. By contrast, cells migrated into the pores of specimen C and covered the surface of the scaffold, which was hardly distinguishable from the nanofibrous matrix. Cell viability on the scaffolds was examined by MTS assay, and the results are shown in Figure 8. Cell viability on the nanofibrous scaffold (specimen C) was significantly better than those on the other three scaffolds. Given that the scaffolds were prepared with the same biomaterial, the topographical morphologies of the scaffolds played a key role in the cell behavior. According to a higher specific surface and structural similarity to natural extracellular matrix (ECM), nanofibrous scaffolds provided a better microenvironment for cells than the solid-walled scaffolds (specimens A and B in this study) and plateletlike scaffold (specimen D in this study).[16,30]

CONCLUSIONS

TIPS is widely used to produce 3D scaffolds for tissue engineering applications. The resulting morphology of the scaffold is affected by various experimental parameters, including the polymer concentration, quenching temperature, rate, quenching period or aging time, solvent-to-nonsolvent ratio, and surfactant or porogen addition. The crystallization behavior of semicrystalline polymers also plays an important role in scaffold morphologies but is seldom given attention. In this study, the crystallization behavior of PLLA in the scaffolds prepared by

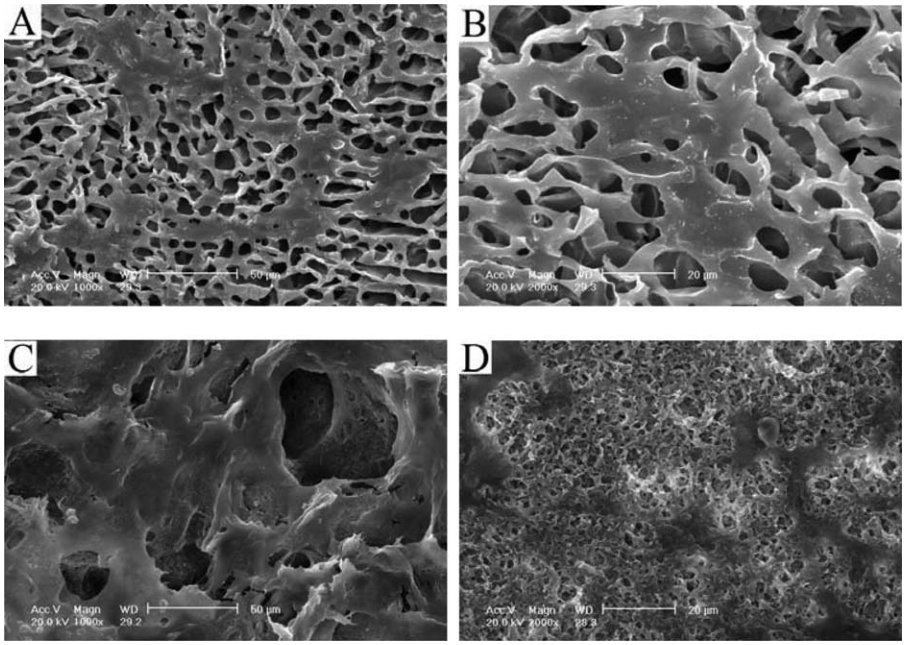

Figure 7. SEM images of NIH-3T3 fibroblasts cultured for 2 days on different scaffolds. Scale bars: (A,C) 50 and (B,D) 20 μm.

four typical TIPS approaches was thoroughly investigated by DSC, XRD, and FTIR spectroscopy.

For all of the PLLA scaffolds fabricated by TIPS from different solvent systems, the DSC, XRD, and IR data on crystallization behavior were highly consistent with one another. The similarity of the characteristics of the XRD patterns and IR spectra of specimen D to those of the PLLA α-form crystal indicated that the α-form crystal was mainly produced in the scaffold from the PLLA–THF binary system at a quenching temperature of 18°C. By contrast, the PLLA α′-form crystal was formed with when the quenching temperature was decreased to −80°C. The PLLA amorphous phase dominated in the scaffolds from the PLLA–dioxane and PLLA–dioxane–water systems, in which the solvent froze when the systems were quenched to a temperature much lower than the freezing point of the solvent. PLLA crystallization competed with phase separation; thus, the crystal structure depended on the complex development of the two processes. In the PLLA–dioxane binary system and the PLLA–dioxane–water ternary system, the solvent immediately froze after quenching to a low temperature; this restricted PLLA chain arrangement and resulted in the amorphous phase, as indicated in the XRD patterns and IR spectra. These amorphous phases contained crystallizable free regions and exhibited a cold-crystallization thermogram in the DSC curves. Porous structures with solid walls were produced from these systems. Given that the freezing point of THF (−80°C) was much lower than the quenching temperature (18°C), the solvent was liquid throughout the entire process; this resulted in more time and freedom for PLLA chain arrangement and crystallization. Further aggregation of single crystals occurred through a crystal nucleation and growth mechanism at T_c = 18°C and resulted in the most common and stable polymorph α form of PLLA. Plateletlike structures were also observed in the scaffold. However, α′-form crystals, proposed to be limit-disordered crystals of α form, were produced at a low T_c (−80°C), and a scaffold with a nanofibrous network was created.

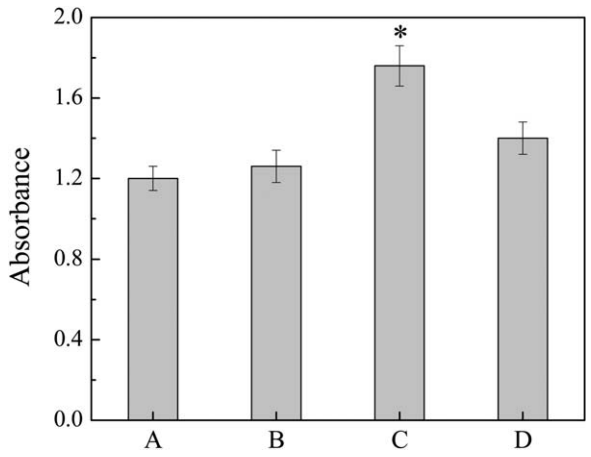

Figure 8. Viability of NIH-3T3 fibroblasts cultured for 2 days on different scaffolds. The asterisk refers to the significant difference between C and the others.

Better cell adhesion and viability were observed in the nanofibrous scaffold than the other three scaffolds; this indicated the advantage of nanofibrous scaffolds over scaffolds of other morphologies.

ACKNOWLEDGMENTS

The authors thank the National Natural Science Foundation of China (contract grant number 51103062) and the Natural Science Foundation of Guangdong Province, China (contract grant number 10451063201005499) for funding support. The authors also

acknowledge the support of the Hong Kong Scholars Program (contract grant number XJ2012024).

REFERENCES

1. Brucato, V.; CarfiPavia, F.; Carrubba, V. L. *Macromol. Symp.* **2009**, *286*, 49.
2. Joachim, K.; Hedrick, J. L.; Hilborn, J. G. *Adv. Polym. Sci.* **1999**, *147*, 161.
3. Zhang, Q.; Zhang, Y.; Xia, D.; Zhao, Y.; Shi, Y.; Jiao, Q. *J. Appl. Polym. Sci.* **2009**, *112*, 1271.
4. Yang, F.; Qu, X.; Cui, W.; Bei, J.; Yu, F.; Lu, S.; Wang, S. *Biomaterials* **2006**, *27*, 4923.
5. Schugens, C.; Maquet, V.; Grandfils, C.; Jerome, R.; Teyssie, P. *Polymer* **1996**, *37*, 1027.
6. Matsuyama, H.; Teramoto, M.; Kuwana, M.; Kitamura, Y. *Polymer* **2000**, *41*, 8673.
7. Tsai, F. J.; Torkelson, J. M. *Macromolecules* **1990**, *23*, 4983.
8. Nam, Y. S.; Park, T. G. *Biomaterials* **1999**, *20*, 1783.
9. Hua, F. J.; Park, T. G.; Lee, D. S. *Polymer* **2003**, *44*, 1911.
10. Shin, K. C.; Kim, B. S.; Kim, J. H.; Park, T. G.; Nam, J. D.; Lee, D. S. *Polymer* **2005**, *46*, 3801.
11. He, L. M.; Zhang, Y. Q.; Zeng, C. G.; Ngiam, M.; Liao, S. S.; Quan, D. P.; Zeng, Y. S.; Lu, J.; Ramakrishna, S. *Tissue Eng. Part C: Methods* **2009**, *15*, 243.
12. Kim, H. D.; Bae, E. H.; Kwon, I. C.; Pal, R. R.; Nam, J. D.; Lee, D. S. *Biomaterials* **2004**, *25*, 2319.
13. Ma, H. Y.; Hu, J.; Ma, P. X. *Adv. Funct. Mater.* **2010**, *20*, 2833.
14. Tao, H. J.; Zhang, J.; Wang, X. L.; Gao, J. L. *J. Polym. Sci. Part B: Polym. Phys.* **2007**, *45*, 153.
15. Ma, P. X.; Zhang, R. *J. Biomed. Mater. Res.* **1999**, *46*, 60.
16. He, L. M.; Zhang, Y. Q.; Zeng, X.; Quan, D. P.; Liao, S. S.; Zeng, Y. S.; Lu, J.; Ramakrishna, S. *Polymer* **2009**, *50*, 4128.
17. Zhang, J.; Duan, Y.; Sato, H.; Tsuji, H.; Noda, I.; Yan, S.; Ozaki, Y.; *Macromolecules* **2005**, *38*, 8012.
18. Chen, J. S.; Tu, S. L.; Tsay, R. Y. *J. Taiwan Inst. Chem. E* **2010**, *41*, 229.
19. Yasuniwa, M.; Tsubakihara, S.; Sugimoto, Y.; Nakafuku, C. *J. Polym. Sci. Polym. Phys.* **2004**, *42*, 25.
20. He, Y.; Fan, Z.; Hu, Y.; Wu, T.; Wei, J.; Li, S. *Eur. Polym. J.* **2007**, *43*, 4431.
21. Pan, P.; Liang, Z.; Zhu, B.; Dong, T.; Inoue, Y. *Macromolecules* **2009**, *42*, 3374.
22. Pan, P.; Zhu, B.; Kai, W.; Dong, T.; Inoue, Y. *J. Appl. Polym. Sci.* **2008**, *107*, 54.
23. Pan, P.; Kai, W.; Zhu, B.; Dong, T.; Inoue, Y. *Macromolecules* **2007**, *40*, 6898.
24. Yasuniwa, M.; Tsubakihara, Y. S.; Iura, K.; Ono, Y.; Dan, Y.; Takahashi, K. *Polymer* **2006**, *47*, 7554.
25. Zhang, J.; Sato, H.; Tsuji, H.; Noda, I.; Ozaki, Y. *J. Mol. Struct.* **2005**, *735–736*, 249.
26. Ribeiro, C.; Sencadas, V.; Costa, C. M.; Ribelles, J. L. G.; Lanceros-Méndez, S. *Sci. Technol. Adv. Mater.* **2011**, *12*, 1.
27. Zhang, J.; Duan, Y.; Domb, A.; Ozaki, Y. *Macromolecules* **2010**, *43*, 4240.
28. Sawai, D.; Takahashi, K.; Sasashige, A.; Kanamoto, T.; Hyon, S. H. *Macromolecules* **2003**, *36*, 3601.
29. Pan, P.; Zhu, B.; Kai, W.; Dong, T.; Inoue, Y. *J. Appl. Polym. Sci.* **2008**, *107*, 54.
30. He, L. M.; Liu, B.; Xie, G. Y.; Liao, S. S.; Quan, D. P.; Cai, D. Z.; Lu, J.; Ramakrishna, S. *Eur. Cells Mater. J.* **2009**, *18*, 63.